OCEANOGRAPHY

Nutrient regulation of biological nitrogen fixation across the tropical western North Pacific

Zuozhu Wen[1]†, Thomas J. Browning[2]†, Yihua Cai[1], Rongbo Dai[1], Ruifeng Zhang[3], Chuanjun Du[1]‡, Ruotong Jiang[1], Wenfang Lin[1], Xin Liu[1], Zhimian Cao[1], Haizheng Hong[1], Minhan Dai[1], Dalin Shi[1]*

Nitrogen fixation is critical for the biological productivity of the ocean, but clear mechanistic controls on this process remain elusive. Here, we investigate the abundance, activity, and drivers of nitrogen-fixing diazotrophs across the tropical western North Pacific. We find a basin-scale coherence of diazotroph abundances and N_2 fixation rates with the supply ratio of iron:nitrogen to the upper ocean. Across a threshold of increasing supply ratios, the abundance of *nifH* genes and N_2 fixation rates increased, phosphate concentrations decreased, and bioassay experiments demonstrated evidence for N_2 fixation switching from iron to phosphate limitation. In the northern South China Sea, supply ratios were hypothesized to fall around this critical threshold and bioassay experiments suggested colimitation by both iron and phosphate. Our results provide evidence for iron:nitrogen supply ratios being the most important factor in regulating the distribution of N_2 fixation across the tropical ocean.

INTRODUCTION

The availability of fixed nitrogen (N) limits primary production throughout most of the global ocean (*1*). Nitrogen fixation by diazotrophic bacteria converts abundant dinitrogen (N_2) gas into ammonia, providing nearly half of the ocean's bioavailable nitrogen (*2*) that goes on to support >30% of carbon export from surface to deep waters in the N-limited ocean (*3*). Furthermore, over geological time scales, the relative balance between N_2 fixation and denitrification controls the marine nitrogen inventory, which has been hypothesized to regulate oceanic carbon sequestration, and thereby atmospheric CO_2 and Earth's climate (*4*–*6*). It follows that how the oceans carbon and nitrogen cycles will respond to future climate change therefore largely depends on how oceanic N_2 fixation responds to environmental change at different spatial-temporal scales (*7*). However, a mechanistic understanding of what controls the distribution of diazotrophs and associated N_2 fixation rates in the current ocean is still lacking, presenting a major barrier to making accurate projections (*8*).

Investigations into the nutritional requirements of diazotrophs have focused on the requirements for iron (Fe) and phosphorus (P), which can be depleted to biologically consequential, very low levels in the surface ocean (*1*). In diazotrophs, Fe demands are elevated relative to nondiazotrophic phytoplankton, due to a major additional requirement as a cofactor for the nitrogenase enzyme (*9*), while diazotrophs share nondiazotroph P requirements for information storage (DNA and RNA) and energy generation [adenosine 5′-triphosphate (ATP)] molecules (*10*). At least conceptually, the ability of diazotrophs to successfully compete with nondiazotrophs and become established in an environment depends on ecological trade-offs between the ability of diazotrophs to fix their own nitrogen on the one hand, with their enhanced Fe requirements and slower growth rates on the other (*11*). This theory accordingly predicts that, in the modern ocean, the external (nondiazotrophic) supply rate of fixed nitrogen, not phosphate, into an ocean ecosystem, relative to that of Fe, is the primary determinant of where diazotrophs occur, with them becoming more successful at elevated Fe:N supply rates (*12*). Within this framework, phosphate on the other hand then sets the critical upper limit on both the overall accumulation of diazotrophs and related magnitude of N_2 fixation that can occur (*12*, *13*). Field evidence for this is, however, largely restricted to a major gradient in Fe supply associated with the Saharan dust plume in the North Atlantic (*14*, *15*).

Suggested controls on N_2 fixation throughout the oligotrophic tropical North Pacific are varied (*16*, *17*). In line with elevated diazotroph Fe requirements, Fe has been hypothesized to limit N_2 fixation in this region due to low level of dust deposition (*13*, *18*, *19*). This is supported by some experimental (*20*) and transcriptomic (*21*) evidence for Fe limitation of N_2 fixation at station ALOHA in the vicinity of Hawaii in the central North Pacific. However, both dust deposition and nutrient concentrations display major zonal gradients across the North Pacific (*22*, *23*), and existing observations of N_2 fixation in the Pacific Ocean show potential for high spatial variability (*8*). A more general framework has been proposed for the Pacific Ocean as a whole, with low Fe inputs to the Eastern Pacific restricting N_2 fixation rates and the drawdown of "excess" upwelled P along eastern boundary currents and the equatorial divergence (*24*), pushing the highest N_2 fixation rates instead to the western Pacific, where much higher dust deposition rates and lower phosphate concentrations have been observed (*3*, *22*, *23*, *25*). However, high rates of N_2 fixation have not been widely documented in the western North Pacific (*26*–*28*). The highest rates observed have been restricted to the western boundary Kuroshio Current, where the "island mass effect" was proposed to provide sufficient Fe and P to this system (*26*, *29*). In the marginal South China Sea (SCS), Fe has been hypothesized to limit the growth of *Trichodesmium* spp., despite high level of dust deposition, due to insufficient Fe-binding organic ligands (*30*). In addition, the nitracline depth, which determines nitrate availability in the upper euphotic layer, has also been hypothesized to regulate *Trichodesmium* spp. abundances in both the northern SCS basin and Kuroshio (*31*). In summary, while

[1]State Key Laboratory of Marine Environmental Science, Xiamen University, Xiamen, Fujian, P. R. China. [2]Marine Biogeochemistry Division, GEOMAR Helmholtz Centre for Ocean Research Kiel, Kiel, Germany. [3]School of Oceanography, Shanghai Jiao Tong University, Shanghai, P. R. China.
*Corresponding author. Email: dshi@xmu.edu.cn
†These authors contributed equally to this work.
‡Present address: State Key Laboratory of Marine Resource Utilization in South China Sea, Hainan University, Haikou, Hainan, P. R. China.

proposed regulation on N_2 fixation rates in this region have been strongly related to nutrient supply, specific controls vary between studies and limited field evidence exists to support an overarching theoretic framework (*12*).

To address this, we carried out a ~8000-km sampling campaign in the tropical western North Pacific, spanning the northern SCS (NSCS), upstream Kuroshio Current, North Pacific Subtropical Gyre (NPSG), and North Equatorial Current (NEC; the southern boundary of NPSG, Fig. 1A). N_2 fixation rates were determined using the $^{15}N_2$ gas dissolution method (*32*), and the abundances of key diazotrophic phylotypes were analyzed via quantification of *nifH* genes. These observations were supported by a diverse range of ancillary environmental parameters, alongside 10 high-volume nutrient amendment experiments directly testing the response of N_2 fixation rates to supply of potentially limiting nutrients (Fe, P, and Fe + P). Our new observational and experimental results match theoretical expectations in revealing the crucial role of Fe:N supply ratios in controlling diazotroph biogeography and associated N_2 fixation rates throughout this ocean basin.

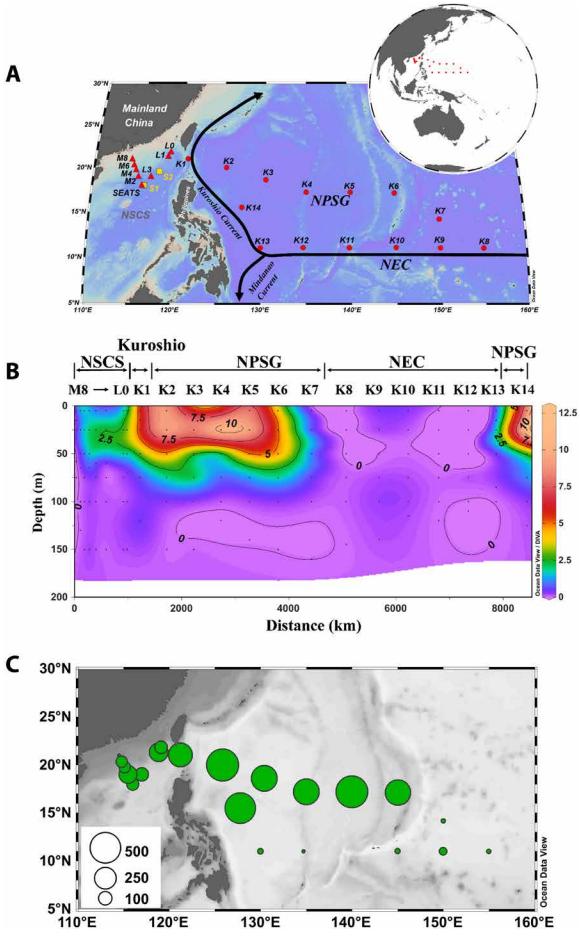

Fig. 1. Distribution of N_2 fixation rates in the tropical western North Pacific. (**A**) Sampling locations: 8 stations (red triangles) were sampled in the northern South China Sea (NSCS) during the MARCO cruise in 2019, and 14 stations (red dots) in the Kuroshio Current (K1), the North Pacific Subtropical Gyre (NPSG; K2 to K7 and K14), and the North Equatorial Current (NEC; K8 to K13) were sampled on the Chinese GEOTRACES-GP09 cruise in 2019. In addition, bioassay incubation experiments were conducted at stations S1 and S2 (yellow squares) on an NSCS cruise in 2018. (**B**) Vertical profiles of N_2 fixation rates (nmol N liter^{-1} day^{-1}). (**C**) Spatial distribution of depth-integrated N_2 fixation (INF; μmol N m^{-2} day^{-1}) for the upper 150-m water column. Note that N_2 fixation rates at stations S1 and S2 were not included in (B) and (C).

RESULTS AND DISCUSSION

Major gradient in N_2 fixation rates

Our survey revealed substantial spatial variability in N_2 fixation rates across the western North Pacific (Fig. 1, B and C). In the NSCS, surface N_2 fixation rates were less than 2.0 nmol N liter^{-1} day^{-1}, and the average depth-integrated N_2 fixation rate was 100 ± 61 μmol N m^{-2} day^{-1} (Fig. 1, B and C, and Table 1), which is twice as high as those reported earlier in the same regions of NSCS measured using the $^{15}N_2$ gas bubble method [~50 μmol N m^{-2} day^{-1}; (*28*, *33*)], but still close to the lower range of 1 to 100 μmol N m^{-2} day^{-1} in the global database (*34*). By contrast, significantly higher rates (3.2 to 9.9 nmol N liter^{-1} day^{-1} and 320 to 573 μmol N m^{-2} day^{-1} for surface and depth-integrated rates, respectively; $P < 0.05$, *t* test) were observed along the large-scale transect from the Kuroshio (station K1) into the NPSG (stations K2 to K6) (Fig. 1, B and C, and Table 1). The Kuroshio Current and its branches have been recognized as "hot spots" of N_2 fixation (*26*, *33*), and thus, it is expected to find high rates in this region. However, in the vast NPSG, relatively higher N_2 fixation rates have previously been observed only at a few stations (*27*, *35*), with an area average rate of ~39 μmol N m^{-2} day^{-1} (*26*). The higher rates observed in our study can potentially be reconciled with a method-derived underestimation of rates in these earlier studies (*32*, *36*). Our new estimates demonstrate the ocean basin–scale occurrence of high diazotroph activity in the oligotrophic NPSG. In contrast, although nitrate concentrations remained fully depleted within the NEC at the southern boundary of the NPSG (fig. S1), we found that N_2 fixation rates declined markedly there to less than 0.42 nmol N liter^{-1} day^{-1} in surface water and to less than 33 μmol N m^{-2} day^{-1} in the upper water column (Fig. 1, B and C, and Table 1).

Spatial variations of diazotroph community structures

All diazotroph groups targeted by the quantitative polymerase chain reaction (qPCR) assay were detected in the study area. Apart from *Trichodesmium*, the *nifH* gene abundances of all groups were elevated in the waters of Kuroshio and NPSG, decreased in the NSCS, and were lowest in the NEC (Fig. 2A). A significant positive correlation was found between the *nifH* gene abundance and N_2 fixation rate (depth-integrated, $R = 0.91$, $P < 0.001$; surface, $R = 0.86$, $P < 0.001$; Fig. 3 and fig. S2), demonstrating that the abundances of these major diazotroph phylotypes well explained the variations in measured rates. However, considerable spatial variation was found in the specific diazotrophs supporting N_2 fixation (Fig. 2).

Trichodesmium was more abundant in the upper 50 m in the NSCS, with a maxima at the surface of station L0 (2.5×10^5 copies liter^{-1}; Fig. 2A). Together, *Trichodesmium* and UCYN-A (A1 and A2/A3) composed ~71% of the total *nifH* gene surveyed in the NSCS (Fig. 2B). These observations were consistent with recent estimates in an adjacent area during the same season (*17*, *33*). Although all of the six diazotroph phylotypes were detected in the NEC, their overall abundances were much lower, in line with the much lower N_2 fixation rates measured there (Figs. 1, B and C, and 2A). The highest N_2 fixation that occurred in the NPSG was driven

Table 1. Ambient environmental conditions and N_2 fixation and primary production rates. Surface seawater temperature (SST), chlorophyll a (Chla), N + N, DIP and dFe concentration, depth of nitracline (D_{Nitr}), 0.1% light level depth (m), surface N_2 fixation rate (SNF), depth-integrated N_2 fixation rate (INF), and primary production (IPP) at each station. nd, no data.

Station	Region	SST (°C)	Chla (μg/liter)	N + N (nM)	DIP (nM)	dFe (nM)	D_{Nitr} (m)	0.1% light level depth (m)	SNF (nmol N liter^{-1} day^{-1})	INF (μmol N m^{-2} day^{-1})	IPP (mmol C m^{-2} day^{-1})
M8	NSCS	30.1	0.184	159	23.5	0.49	5	82	0.27*	5*	42
M6	NSCS	30.1	0.106	61	18.2	0.62	10	nd	1.81	73	44
M4	NSCS	30.7	0.114	122	20.5	0.67	5	100	1.89	73	41
M2	NSCS	30.7	0.090	46	17.4	0.43	37	nd	1.24	178	32
SEATS	NSCS	30.7	0.121	47	17.9	0.27	51	100	0.79	83	17
L3	NSCS	30.4	0.123	12	13.9	nd	26	99	1.00	100	33
L1	NSCS	29.6	0.132	33	16.4	nd	51	104	2.02	196	72
L0	NSCS	30.3	0.096	42	14.5	0.28	50	128	1.37	92	54
K1	Kuroshio	28.3	0.038	5.1†	25.2	0.25	101	144	6.03	320	31
K2	NPSG	29.1	0.035	2.0†	37.4	0.34	131	149	9.89	573	24
K3	NPSG	28.8	0.035	2.3†	27.1	0.21	158	151	5.11	375	21
K4	NPSG	29.8	0.025	8.1	26.5	0.30	105	153	5.15	373	23
K5	NPSG	29.3	0.025	2.3†	32.8	0.25	143	148	9.85	559	26
K6	NPSG	29.8	0.026	5.7†	35.0	0.27	171	163	3.24	360	19
K7	NPSG	29.5	0.017	10.1	50.1	0.31	151	167	0.00*	10*	13
K8	NEC	29.1	0.025	5.5†	131.9	0.23	133	157	0.06*	11*	17
K9	NEC	29.6	0.030	2.6†	93.6	0.22	83	164	0.42	33	18
K10	NEC	29.6	0.026	8.1	76.6	0.24	123	157	0.26*	16*	18
K11	NEC	29.8	0.045	4.8†	64.7	0.20	80	160	0.00*	0*	21
K12	NEC	30.0	0.037	5.1†	63.4	0.19	75	130	0.00*	7*	16
K13	NEC	29.9	0.041	4.6†	35.5	0.19	54	127	0.23*	20*	13
K14	NPSG	30.5	ND	2.3†	12.2	0.22	123	148	8.93	521	27

*Below detection limit. Taking 4‰ as the minimum acceptable change in the $\delta^{15}N$ of particulate nitrogen (*50*). †Below the limit of quantification (N + N = 7.46 nM; DIP = 4.2 nM).

by unicellular cyanobacteria diazotrophs (Fig. 2B), consistent with a previous study in this region demonstrating that nanoplanktonic cyanobacteria (<10 μm) were responsible for the major portion of N_2 fixation (*37*). Furthermore, similar results obtained by qPCR assays and *nifH* gene sequencing have been reported elsewhere in the Pacific (*38*–*40*). Our observations therefore contribute toward increasing evidence for the fundamental role of unicellular cyanobacterial diazotrophs in maintaining elevated N_2 fixation in the ultra-oligotrophic ocean (*41*). However, a difference in our study was the dominant type of unicellular diazotrophs found. Previous studies found UCYN-A to be the most dominant cyanobacteria diazotroph in the central and eastern Pacific (*38*–*40*). In contrast, we found that UCYN-B composed 64 to 92% of total *nifH* gene copies in the western NPSG (Fig. 2B), which was ~2 to 14 times higher than the abundance of UCYN-A (table S2). This difference may be attributed to the specific niches of UCYN-A and UCYN-B. For example, warmer seawater is more favorable to UCYN-B (27° to 29°C), while UCYN-A prefers temperate environments [24° to 25°C; (*38*, *42*)]. In our study, UCYN-B abundance was positively correlated with temperature in the western North Pacific (R^2 = 0.12 and P < 0.01; fig. S3), while a significant negative correlation was found with UCYN-A (R^2 = 0.39 and P < 0.01; fig. S3). Thus, surface temperatures around 29°C (in the range of 28.3° to 30.5°C; Table 1 and fig. S1) characterizing the western North Pacific were more favorable for the growth of UCYN-B, while UCYN-A was more abundant in the regions and seasons when temperatures are cooler (*38*–*40*). In addition, these interspecies differences in optimum temperatures can also potentially explain why UCYN-A was mainly restricted to depths between 50 and 100 m, while UCYN-B was homogeneously distributed in the upper 75 m (Fig. 2A).

Fe:N supply rate predicts diazotroph biogeography and nutrient limitation patterns

No significant correlations were found between surface or depth-integrated N_2 fixation rates and sea surface temperatures, nitrate + nitrite (N + N), phosphate (DIP), or dissolved Fe (dFe) concentrations (Fig. 3). This demonstrated that residual nutrient concentrations were neither good predictors nor the driving factors of the broad-scale variations in N_2 fixation rates that we observed across this system. In contrast to standing concentrations, resource competition theory instead predicts that diazotrophs will successfully compete with nondiazotrophs at elevated Fe:N supply rates, where the burden of additional diazotroph Fe requirements is compensated by their ability to fix N_2 (*11*, *12*). For the open ocean stations (K1 to K14),

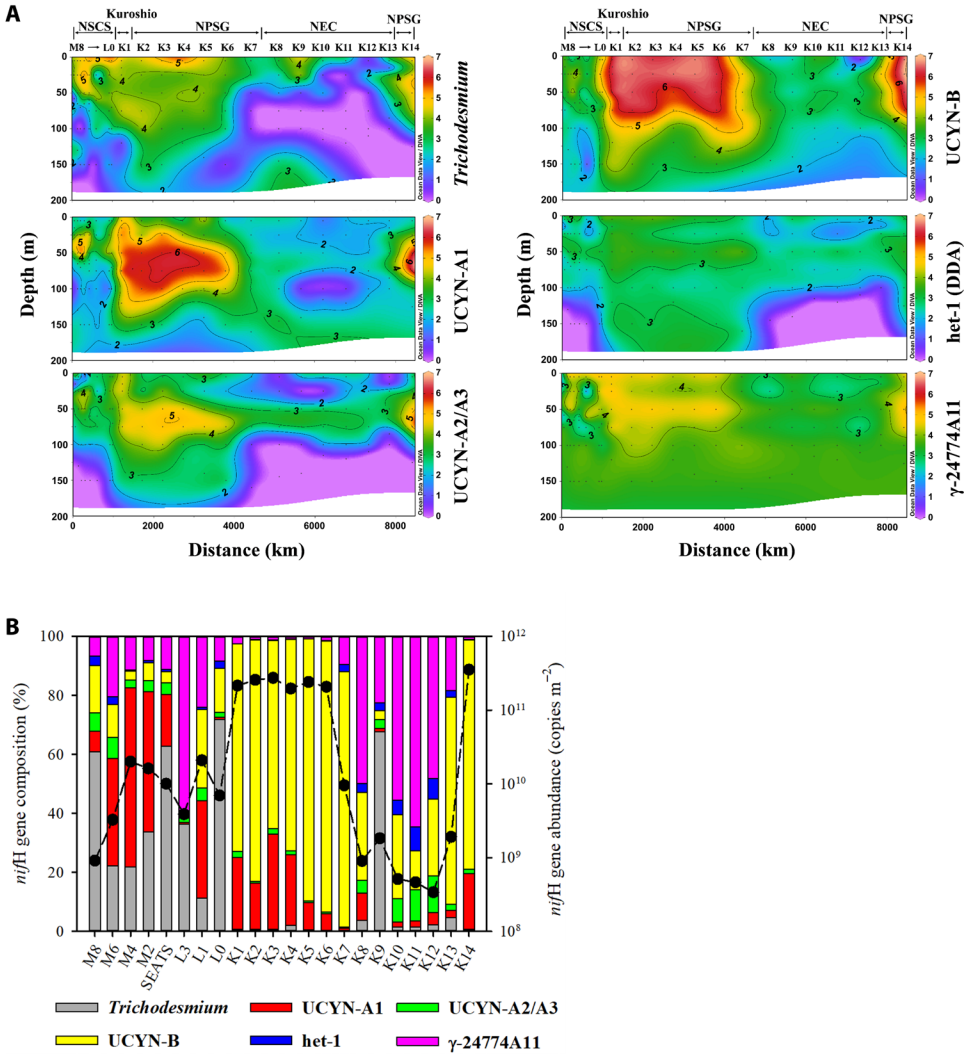

Fig. 2. qPCR-based *nifH* gene abundance and composition in the tropical western North Pacific. (**A**) Vertical distributions of diazotrophs [$\log_{10}$ (copies liter^{-1})]. (**B**) *nifH* gene composition of six target diazotrophs. Depth-integrated *nifH* gene abundance (the black dots) was used for the proportion calculation of each group.

where water column profiles of both nitrate and dFe were available, we estimated the turbulent diffusive supply of both nutrients into the euphotic zone (in this study defined as the 0.1% light level). We then added these subsurface supply rates with aerosol deposition rates predicted by a global model (*43*) to derive an overall estimate of the Fe:N supply ratio to the surface, sunlit ocean layer (Materials and Methods). In contrast to standing concentrations, we find that the derived Fe:N supply ratio shows a clear spatial coherence with both depth-integrated N_2 fixation rates and *nifH* abundances (Fig. 4A and fig. S4), with elevated values for NPSG stations and low values around the NEC where (i) Ekman divergence shoals the nitracline upward to the euphotic depth, enhancing turbulent nitrate supply from below, and (ii) aerosol Fe supply from above is reduced. In the NSCS, where depth profiles of dFe were not available, we hypothesize that elevated Fe supply from aerosols and shelf sediments is balanced by elevated nitrate supply from shoaled nitraclines (Fig. 5), stimulating overall enhanced primary production in this region (Fig. 5 and fig. S5) and generating Fe:N supply ratios and hence diazotroph abundances and N_2 fixation rates falling in between NEC and NPSG values.

Our field observations of spatial patterns in diazotrophs and N_2 fixation rates matching Fe:N supply ratios strongly align with previously proposed resource competition theory (*11*), which is encapsulated within a simple numerical model simulating the competition between diazotrophs and nondiazotrophs [Fig. 4, B and C, and (*12*)]. The spatial variability we observe in calculated Fe:N supply ratios in the western subtropical North Pacific (Fig. 4) is predominantly driven by spatial gradients in nitracline depths and aerosol Fe deposition, with generally deeper nitraclines and enhanced aerosol Fe in the northern NPSG stations increasing the Fe:N supply ratio relative to southern NEC stations (table S3). Reproducing this trend in the model by forcing it with an increasing supply ratio of Fe:N via (i) progressively reducing the subsurface nitrate concentration and (ii) increasing aerosol Fe deposition, the model predicts that diazotrophs switch from being competitively excluded to becoming more abundant across a critical threshold Fe:N supply ratio

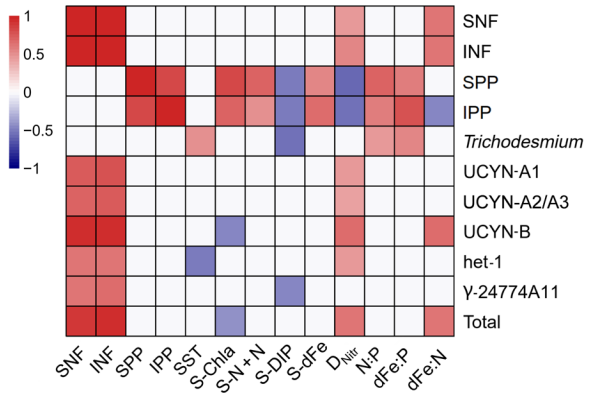

Fig. 3. Pairwise correlations between N_2 fixation rates, depth-integrated diazotroph abundances, and environmental factors. Color gradient denotes Pearson correlation coefficients. Only the significant correlations ($P \leq 0.05$) are colored, and the whites indicate $P > 0.05$. SNF, surface N_2 fixation rate; SPP, surface primary production; IPP, depth-integrated primary production; SST, surface sea temperature; S-Chla, surface chlorophyll a concentration; S-N + N, surface nitrate plus nitrite concentration; S-DIP, surface phosphate concentration; S-dFe, surface dFe concentration; D_{Nitr}, depth of nitracline; N:P, dFe:P and dFe:N are ratios of surface nutrient concentrations. Depth-integrated *nifH* gene abundance of each diazotroph phylotypes is used in correlation analysis, and Total represents total *nifH* gene abundance of six diazotrophs that surveyed.

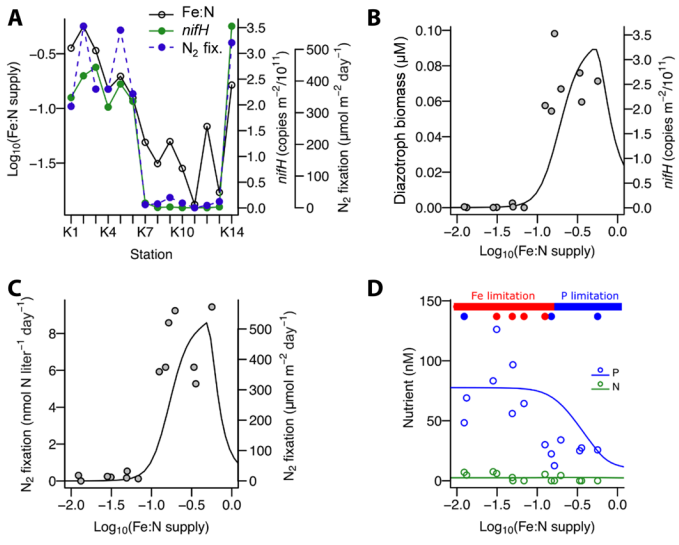

Fig. 4. Regulation of diazotrophs and N_2 fixation by Fe:N supply ratios. (**A**) Basin-scale coherence of calculated Fe:N supply rates, derived from vertical turbulent diffusion and model aerosol deposition, with depth-integrated *nifH* and N_2 fixation rates. (**B** and **C**) Outcome of a resource competition model under increasing Fe:N supply rates (lines), with observations overplotted (gray points). (**D**) Changes in steady-state phosphate and nitrate concentrations in the model (lines), with observations overplotted (symbols; concentrations are those averaged over the upper 50-m water column depth). The solid red and blue bars indicate where the model diazotrophs are limited by Fe and P, respectively; filled symbols below indicate the limiting nutrient for N_2 fixation found in the bioassay experiments (Fig. 6).

(*11*), with this threshold-type response closely matching our field observations (Fig. 4, B and C). Although less clear than for the calculated Fe:N supply rate ratios, we also find a relationship between N_2 fixation rates and the surface dFe:N concentration ratio ($R = 0.62$, $P = 0.003$; Fig. 3), again matching the theoretical expectation that the residual concentration ratio of these nutrients will to some extent reflect the supply ratio at steady state (*11*).

In line with previous observations across the well-studied (sub) tropical Atlantic, where a major gradient in Saharan aerosol Fe deposition drives a sudden switch in Fe:N supply rates (*14*, *15*, *44*), our analysis suggests that variations in nitracline depths in conjunction with aerosol deposition are a similarly crucial determinant of where diazotrophs become established in the western tropical North Pacific. In alignment with resource competition theory (*44*), we suggest that this is via their dominant control on the Fe:N supply ratio in this system. Other hypotheses could be formulated to attribute direct control of diazotroph biogeography by the nitracline depth, or N supply rates alone (i.e., independent of changes in Fe supply rates; Fig. 3), which likely affects other ecosystem processes not taken into account within the relatively simple resource competition framework used here (e.g., by driving changes in phytoplankton communities with different physiologies and mortalities). However, the latter would suggest different controls on broad-scale patterns of diazotroph distributions in the (sub)tropical Pacific and Atlantic (*14*, *44*). Furthermore, such hypotheses would be inconsistent with the intermediate levels of diazotrophs that we found in the NSCS (Fig. 1C), where the nitracline is much shallower than the NEC (Table 1).

In addition to diazotroph biomass levels (here estimated by *nifH*), our dataset further suggests that the control of Fe:N supply ratios on diazotroph biomass levels (here estimated by *nifH*) is also the overriding control on measured N_2 fixation rates, as they strongly correlate (Fig. 3 and fig. S2). The resource competition model used here also makes predictions on the subsequent proximal limiting nutrient for N_2 fixation rates in each part of the system (Fig. 4D). Specifically, where the Fe:N supply ratio is low, the low-level diazotroph population is predicted to be Fe limited (while the nondiazotrophs can remain N limited), whereas under elevated Fe:N supply ratios where diazotrophs become well established, P begins to be drawn down and replaces Fe as the resource limiting to N_2 fixation.

We found that the N_2 fixation limitation patterns that emerged in the resource competition model were broadly consistent with what was observed in the field (Fig. 6). To the best of our knowledge, we conducted the first experimental assessments of nutrient limitation of N_2 fixation throughout the tropical western North Pacific: 10 large-volume (10-liter) bioassay experiments were conducted, where seawater was amended with P, Fe, or Fe + P and N_2 fixation rates were determined following 3-day incubation (Fig. 6). In the south eastern region, characterized by low Fe:N supply, standing phosphate concentrations were generally elevated (50 to 132 nM) and N_2 fixation rates increased only following addition of Fe (stations K6 to K8 and K12; Fig. 6). In contrast, within the northwest NPSG that was characterized by elevated Fe:N supply, phosphate concentrations were reduced (12 to 37 nM) and N_2 fixation rates increased significantly following supply of P (stations K2 and K4; Fig. 6). Some exceptions to these trends were found. First, in the single station located in the Kuroshio Current (station K1), P and/or Fe addition led to no enhancement of N_2 fixation rates, suggesting that factors other than nutrient availability were regulating N_2 fixation rates at this site (Fig. 6). Second, at station K13, located in the NEC where low Fe:N supply rates were calculated, we observed

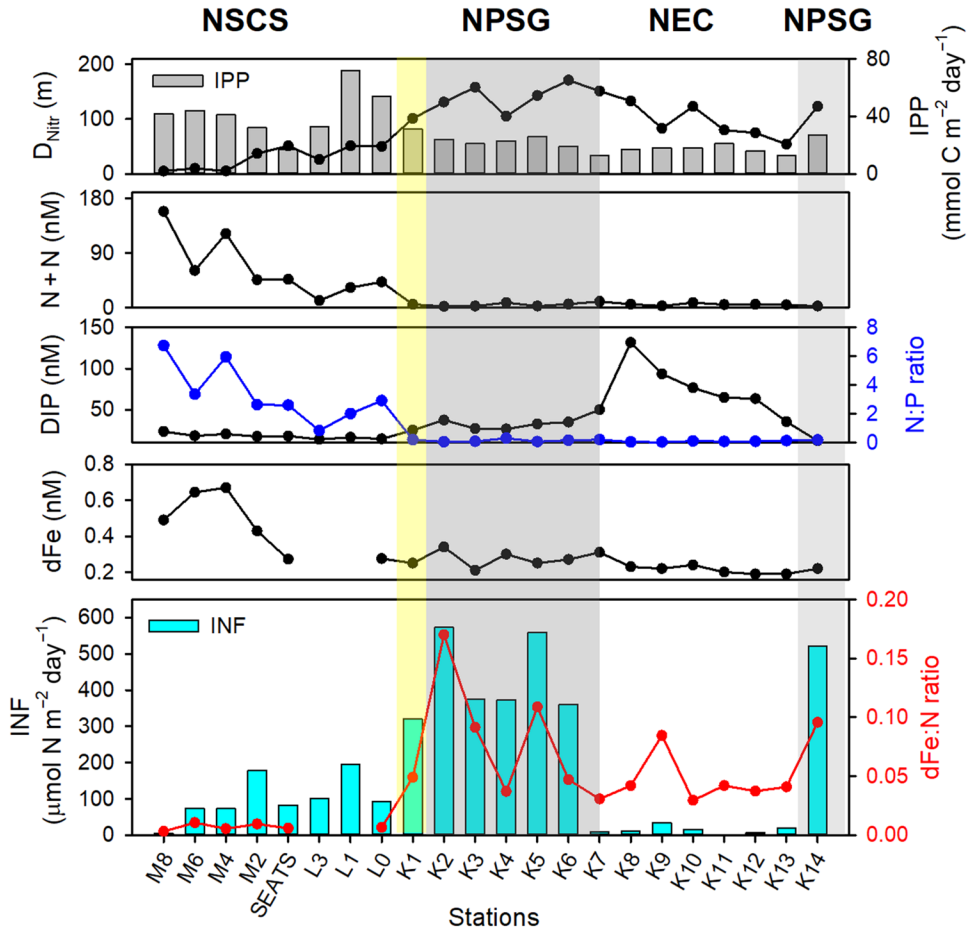

Fig. 5. The controls of N_2 fixation rates in the western North Pacific. Distribution of INF, IPP, and environmental factors including D_{Nitr}, surface N + N, DIP and dFe concentration, and surface N:P and dFe:N concentration ratios in the study area. The yellow shadow indicates Kuroshio station, and the gray shadows indicate NPSG stations.

relatively depleted phosphate (35 nM) and significant increases in N_2 fixation rates only followed supply of P.

In addition to Fe limitation at low Fe:N supply and P limitation at elevated Fe:N supply, the resource competition model predicts that at values around the threshold Fe:N supply ratio, diazotrophs approach colimitation by both Fe and P [Fig. 4D and (*45*)]. True colimitation is not possible in the simple numerical model, as the limiting resource switches instantaneously from Fe to P (Fig. 4). However, at least for nondiazotrophic phytoplankton, a range of mechanisms have been proposed to broaden the extent of colimitation at nutrient limitation transition boundaries, including enhanced diversity in microbial requirements for different nutrients and abilities to access different chemical forms of these nutrients (*46*). In the NSCS region, although residual surface dFe concentrations were elevated (Table 1 and Fig. 5) and phosphaclines shallow (fig. S1), N_2 fixation rates were only significantly enhanced following combined P and Fe supply (stations S1 and S2; Fig. 6), demonstrating that rates were colimited by both nutrients (*45*). In addition to adding evidence for the potentially widespread nature of Fe-P colimitation of N_2 fixation under elevated Fe supply (*15*, *45*), this colimitation situation further matches our hypothesis that the intermediate diazotroph abundances and N_2 fixation rates observed at the NSCS sites were driven by the outcome of competition with nondiazotrophs at intermediate Fe:N supply rates (Fig. 4).

In conclusion, by carrying out a large spatial scale investigation of diazotrophs and N_2 fixation rates and linking this to established resource competition theory, we present a framework for understanding controls on marine N_2 fixation in the tropical western North Pacific. As Fe:N supply rates increase due to deepening nitraclines and increasing aerosol Fe deposition, a threshold is reached where diazotrophs are sufficiently competitive to coexist with nondiazotrophs and N_2 fixation rates increase. This, in turn, leads to a drawdown in phosphate concentrations. Contrary to recent suggestions by numerical model studies that N_2 fixation in the western North Pacific is under P limitation (*47*) or nutrient-replete condition (*3*), our study demonstrates that across this threshold the proximal limiting nutrient for N_2 fixation switches from Fe to phosphate. Thus, our field observations support the hypothesis that phosphate availability sets an upper bound on how much N_2 fixation can occur in this system, while the supply ratio of Fe:N is currently the main determinant of spatial basin-scale patterns in N_2 fixation rates. This alignment with theoretical expectations has important implications for predicting N_2 fixation at ocean basin scales and projecting how it will change under future environmental perturbation.

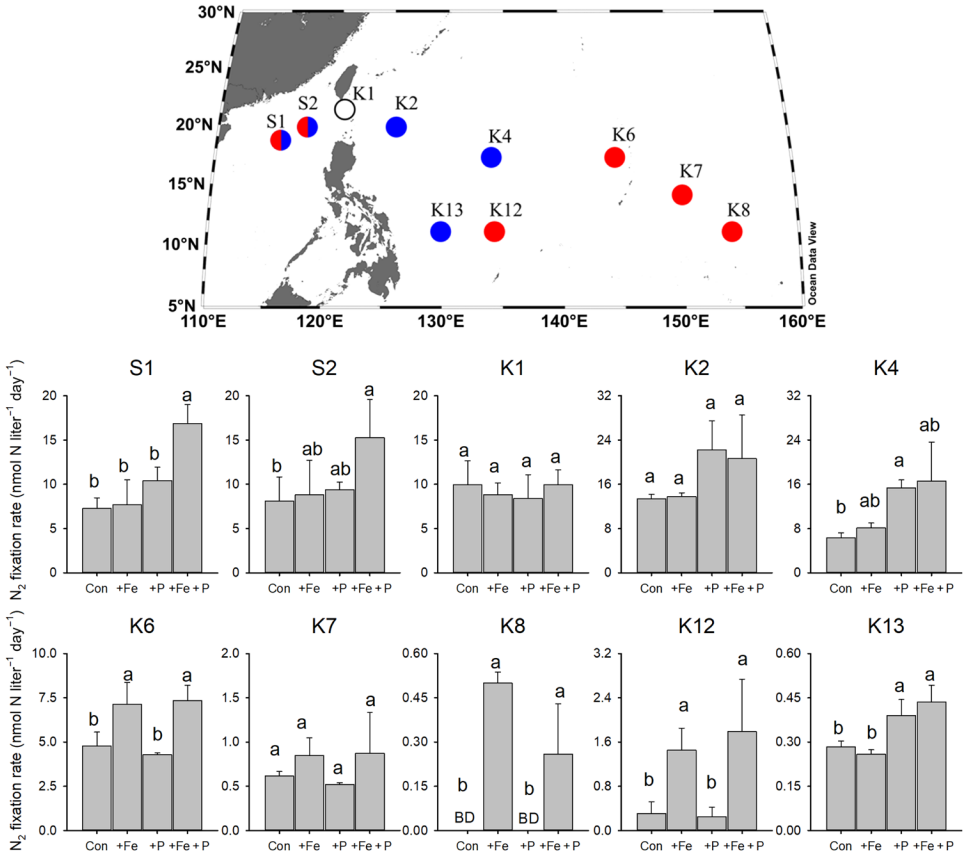

Fig. 6. Response of N_2 fixation to nutrient addition. Symbols summarize the nutrient limitation of N_2 fixation found at each site: red, Fe limitation; blue, P limitation; split red/blue, Fe-P colimitation; white, Fe and P replete. Con, control; +Fe, 2 nM; +P, 100 nM; +Fe + P, both Fe and P were added. Error bars represent the SD of biological replicates ($n = 3$). BD stands for values below detection limit. Different letters above error bars indicate statistically significant difference ($P < 0.05$) between treatments (ANOVA followed by Tukey test).

MATERIALS AND METHODS

Sample collection

All the investigations and most of the bioassay experiments were conducted on the Chinese GEOTRACE-GP09 (from 25 April to 13 June) and MARCO (17 June to 5 July) cruises onboard the R/V *Tan Kah Kee* in 2019. Two bioassay experiments (at stations S1 and S2, Fig. 1A) were conducted on an NSCS cruise from 2 June to 11 August in 2018 on the same vessel. At each station shown in Fig. 1A, temperature and salinity were recorded by a Seabird 911 CTD. Water samples were collected using Niskin-X bottles at six depths throughout the upper 150 m for the determination of *nifH* gene abundance and for N_2 fixation and primary production incubations. Samples for nutrient analysis were collected throughout the upper 200 m. Seawater samples for dFe and for the bioassay experiments were collected either using trace-metal-clean Niskin-X bottles or using a trace-metal-clean towed sampling device located around 2 to 5 m depth, with suction provided by a Teflon bellows pump (*48*). Seawater was sampled in a dedicated trace-metal-clean sampling container maintained overpressurized by high-efficiency particulate air (HEPA)–filtered air.

N_2 fixation and primary production measurements

N_2 fixation rates were determined by the $^{15}N_2$ gas dissolution method (*32*), combined with a primary production assay using $NaH^{13}CO_3$ (99 atom % ^{13}C, Cambridge Isotope Laboratories). The $^{15}N_2$ predissolved seawater was made with $^{15}N_2$ gas (98.9 atom %, Cambridge Isotope Laboratories) according to Shiozaki *et al.* (*49*). Briefly, 0.22-μm filtered seawater was degassed using a Sterapore membrane unit (20M1500A: Mitsubishi Rayon Co. Ltd., Tokyo, Japan). After that, 20 ml of $^{15}N_2$ gas was injected into a gas-tight plastic bag containing 2 liters of the degassed seawater and allowed to fully equilibrate before use. The N_2 fixation and primary production incubations were conducted in duplicate 2.3- or 4.5-liter Nalgene polycarbonate bottles. Samples were spiked with 50 or 100 ml of $^{15}N_2$-enriched filtered seawater from the same site and incubated on-deck for 24 hours. The final $^{15}N_2$-enriched seawater concentration in the incubation bottles was not measured directly during this study. In a following cruise in winter 2020 to the same region in the NPSG as this study, we sampled the $^{15}N_2$ atom % directly from the N_2 fixation incubation bottles, which were conducted using exactly the same approach, reagents, and equipment as for the study described here. Measurements were conducted using membrane inlet mass spectrometry (MIMS), and the $^{15}N_2$ atom% in the incubation bottles showed low variation ranging from 1.28 to 1.56 atom % (table S1), with a mean ± SD of 1.40 ± 0.08 atom % ($n = 17$). Given the stability of our methods, this average value of 1.4 atom % $^{15}N_2$ enrichment was used to calculate N_2 fixation rates of this study. For primary production rate measurements, $NaH^{13}CO_3$ solution was

added at a concentration of 100 μM. After that, the bottles were covered with neutral-density screen to adjust the light to the levels at sampling depths, and then were incubated for 24 hours in an on-deck incubator continuously flushed with surface seawater. Incubated samples were filtered onto precombusted (450°C, 4 hours) GF/F filters, and the particulate organic matter from each depth was also collected to determine background ^{15}N-PON and ^{13}C-POC natural abundances. All filter samples were acid-fumed to remove the inorganic carbon and then analyzed using an elemental analyzer coupled to a mass spectrometer (Flash HT 2000-Delta V Plus, Thermo Fisher Scientific). The N_2 fixation and primary production rates were then calculated according to Montoya *et al.* (*50*) and Hama *et al.* (*51*), respectively. The detection limits of N_2 fixation rates were then calculated according to Montoya *et al.* (*50*), taking 4‰ as the minimum acceptable change in δ^{15}N of particulate nitrogen. All parameters involved in N_2 fixation rate calculation are shown in data S1. To represent the inventories, the upper 100-m depth-integrated N_2 fixation rate and primary production were calculated by the trapezoidal integration method.

nifH gene abundance

Four liters of seawater samples for DNA extractions was filtered onto 0.22-μm pore-sized membrane filters (Supor 200, Pall Gelman, NY, USA) and then frozen in liquid N_2. To extract the DNA, membranes were cut into pieces under sterile conditions and then extracted using the QIAamp DNA Mini Kit (Qiagen) following the manufacturer's protocol. The qPCR analysis was targeted on the *nifH* phylotypes of *Trichodesmium* spp.; unicellular cyanobacterial UCYN-A1, UCYN-A2, and UCYN-B; *Richelia* spp. (het-1); and a gamma-proteobacterium (γ-24774A11), using previously designed primers and probe sets [table S4; (*52*–*55*)]. A recent study suggested that the primers for UCYN-A2 also target UCYN-A3 and thus cannot be used to differentiate between these two phylotypes (*56*). Therefore, we used the convention UCYN-A2/A3 when referring these two groups. The *nifH* standards were obtained by cloning the environmental sequences from previous samples collected from the SCS. qPCR analysis was carried out as described previously (*52*) with slight modifications. Triplicate qPCRs were run for each environmental DNA sample and for each standard on the CFX96 Real-Time System (Bio-Rad Laboratories). Standards corresponding to between 10^1 and 10^7 copies per well were amplified in the same 96-well plate. The amplification efficiencies of PCR were always between 90 and 105%, with R^2 values >0.99. The quantification limit of the qPCRs was 10 *nifH* gene copies per reaction, and 1 μl from 100 μl of template DNA was applied to qPCR assay, which was equivalent to approximately 250 gene copies per liter of seawater sample filtered (4 liters).

Bioassay experiments

Acid-cleaned Nalgene polycarbonate carboys (10 liters) were filled with near-surface seawater from the towed fish system. Trace-metal-clean techniques were strictly applied in experimental setup and manipulations. All materials coming in contact with the incubation water were acid-cleaned in a Class-100 cleanroom before use. Nutrient amendments at all sites were Fe, P, and Fe + P. The amended Fe and P (chelexed and filter-sterilized) concentrations were 2 and 100 nM, respectively. Control bottles incubated with no nutrient treatment were included with all experiments. All treatments were conducted with triplicate replicates and incubated for 3 days in a screened on-deck incubator continuously flushed with surface seawater. After preincubation, subsamples were collected for the determination of N_2 fixation rate. $^{15}N_2$-enriched seawater was prepared as described above, except that all the materials coming in contact with the seawater were acid-cleaned before use.

Macronutrient and trace element analyses

Samples for macronutrient analyses were collected in 125-ml acid-washed high-density polyethylene bottles (Nalgene) and analyzed onboard using the Four-channel Continuous Flow Technicon AA3 Auto-Analyzer (Bran-Lube GmbH). The detection limits for NO_3^-, NO_2^-, and DIP were 0.03, 0.02, and 0.03 μM, respectively. Low-level DIP concentrations were determined onboard following Ma *et al.* (*57*), and low-level nitrate + nitrite (N + N) concentrations were determined on frozen (−20°C) samples following Zhang (*58*).

Samples of the dFe concentration of the GEOTRACE-GP09 cruise were collected using a GEOTRACES-standard trace-metal-clean rosette with Niskin-X bottles and analyzed by chemiluminescence-based flow injection following King *et al.* (*59*) after preconcentration by an inline PA-1 column. We determined the following dFe concentrations for the SAFe seawater reference materials: 0.091 ± 0.01 nM (n = 6) for SAFe seawater reference material S, 0.65 ± 0.03 nM (n = 6) for SAFe seawater reference material D1, and 0.987 ± 0.047 nM (n = 8) for SAFe seawater reference material D2. These values compare well with community consensus concentrations of 0.093 ± 0.008, 0.67 ± 0.04, and 0.993 ± 0.023 nM, respectively. Samples from the MARCO cruise were collected using the towed fish system described above, and dFe was measured using an offline seaFAST pico method (Elemental Scientific Inc.). Seawater samples (10 ml) were amended with a ^{57}Fe isotope spike, processed according to a preprogrammed routine (*60*), and then analyzed on a reaction/collision cell triple-quadrupole inductively coupled plasma mass spectrometry (iCAP TQ, Thermo Fisher Scientific), with NH_3 as reaction gas to remove ArO interference on ^{56}Fe.

Nutrient supply rates and ratios

The subsurface supply rate of nitrate and dFe into the euphotic zone (here defined as the 0.1% light level; Table 1) was calculated using vertical profiles of these nutrients and a turbulent diffusivity constant. Nutrient profiles were first interpolated at 1-m vertical resolution, and then the gradient between the mean nutrient concentration 10 m above and 10 m below the euphotic zone was calculated. Nutrient gradients were multiplied by a typical open ocean turbulent diffusivity constant [1×10^{-5} m^2 s^{-1}; e.g., (*61*)]. In the case of one calculation of a negative gradient (for Fe), we assumed an upward turbulent diffusion of zero. The calculated turbulent nutrient supply depends on (i) the specific depth chosen to calculate the nutrient gradient and (ii) our assumption of a constant turbulent diffusivity constant. Both will affect the exact value of calculated Fe:N supply ratios and therefore the specific ratio separating where diazotrophs were and were not established (Fig. 4A). Aerosol supply rates of nitrate + ammonium and soluble Fe were extracted from the published model result of Chien *et al.* (*43*) for an April-May-June average for model grid cells matching station locations. This model simulates wet and dry nutrient deposition and includes fire emissions [a full model description is available in the study of Chien *et al.* (*43*)]. Subsurface and aerosol supply rates of N and Fe were added together for each station, and then an overall Fe:N

supply rate ratio was calculated. The contribution of each term to the Fe:N supply ratio is shown in table S3.

Resource competition model

The resource competition model of Ward *et al.* (*12*) and Schlosser *et al.* (*44*) was used to demonstrate the expected outcome of competition between diazotrophs and nondiazotrophs under varying Fe:N supply rates. In the model, N, P, and Fe are supplied from the subsurface (for instance, reflecting waters just below the euphotic zone), with the supply rate being dictated by the prescribed concentration of these nutrients in the subsurface and a fixed mixing coefficient. Aerosols were assumed to supply Fe only. Nondiazotrophs and diazotrophs then compete for these resources under grazing pressure (constant mortality term). Diazotrophs are assumed to be able to fix all the N they require but have higher Fe and P requirements and slower growth rates than nondiazotrophs. To vary the Fe:N supply rate from low to high values (Fig. 4), the prescribed N concentration of subsurface waters was reduced, while aerosol Fe was simultaneously increased. This matches the gradients between southern NEC stations and northern NPSG stations in our study region. At each supply rate ratio, the model was run to steady state (unvarying phytoplankton/nutrient concentrations) and the model output was extracted (Fig. 4, B to D). Model parameters were largely similar to those detailed by Ward *et al.* (*12*), but some were modified so that the critical Fe:N supply ratio threshold between no diazotrophy to diazotrophy matched the field observations. Model parameters and variables used are shown in table S5.

Statistical analysis

Significance of differences among oceanic regions (for N_2 fixation rate and *nifH* gene abundance) and among nutrient treatments of bioassay experiments (for N_2 fixation rate) were tested by *t* test and analysis of variance (ANOVA) followed by Tukey test, respectively, using SigmaPlot 12.5. Pairwise correlation between N_2 fixation rates, diazotroph groups, and environmental factors was analyzed using Pearson correlation. A significance level of $P < 0.05$ was applied, except as noted where significance was even greater.

SUPPLEMENTARY MATERIALS

Supplementary material for this article is available at https://science.org/doi/10.1126/sciadv.abl7564

REFERENCES AND NOTES

1. C. M. Moore, M. M. Mills, K. R. Arrigo, I. Berman-Frank, L. Bopp, E. D. Galbraith, R. J. Geider, C. Guieu, S. L. Jaccard, T. D. Jickells, J. La Roche, T. M. Lenton, N. M. Mahowald, E. Marañón, I. Marinov, J. K. Moore, T. Nakatsuka, A. Oschlies, M. A. Saito, T. F. Thingstad, A. Tsuda, O. Ulloa, Processes and patterns of oceanic nutrient limitation. *Nat. Geosci.* **6**, 701–710 (2013).
2. N. Gruber, J. N. Galloway, An Earth-system perspective of the global nitrogen cycle. *Nature* **451**, 293–296 (2008).
3. W. L. Wang, J. K. Moore, A. C. Martiny, F. W. Primeau, Convergent estimates of marine nitrogen fixation. *Nature* **566**, 205–211 (2019).
4. M. A. Altabet, Constraints on oceanic N balance/imbalance from sedimentary ^{15}N records. *Biogeosciences* **4**, 75–86 (2007).
5. P. G. Falkowski, Evolution of the nitrogen cycle and its influence on the biological sequestration of CO_2 in the ocean. *Nature* **387**, 272–275 (1997).
6. A. F. Michaels, D. M. Karl, D. G. Capone, Element stoichiometry, new production and nitrogen fixation. *Oceanography* **14**, 68–77 (2001).
7. L. Wrightson, A. Tagliabue, Quantifying the impact of climate change on marine diazotrophy: Insights from Earth System Models. *Front. Mar. Sci.* **7**, 635 (2020).
8. W. Tang, Z. Li, N. Cassar, Machine learning estimates of global marine nitrogen fixation. *Eur. J. Vasc. Endovasc. Surg.* **124**, 717–730 (2019).
9. I. Berman-Frank, J. T. Cullen, Y. Shaked, R. M. Sherrell, P. Falkowski, Iron availability, cellular iron quotas, and nitrogen fixation in *Trichodesmium*. *Limnol. Oceanogr.* **46**, 1249–1260 (2001).
10. D. M. Karl, Microbially mediated transformations of phosphorus in the sea: New views of an old cycle. *Annu. Rev. Mar. Sci.* **6**, 279–337 (2014).
11. S. Dutkiewicz, B. A. Ward, J. R. Scott, M. J. Follows, Understanding predicted shifts in diazotroph biogeography using resource competition theory. *Biogeosciences* **11**, 5445–5461 (2014).
12. B. A. Ward, S. Dutkiewicz, C. M. Moore, M. J. Follows, Iron, phosphorus, and nitrogen supply ratios define the biogeography of nitrogen fixation. *Limnol. Oceanogr.* **58**, 2059–2075 (2013).
13. J. Wu, W. Sunda, E. A. Boyle, D. M. Karl, Phosphate depletion in the western North Atlantic Ocean. *Science* **289**, 759–762 (2000).
14. C. M. Moore, M. M. Mills, E. P. Achterberg, R. J. Geider, J. LaRoche, M. I. Lucas, E. L. McDonagh, X. Pan, A. J. Poulton, M. J. A. Rijkenberg, D. J. Suggett, S. J. Ussher, E. M. S. Woodward, Large-scale distribution of Atlantic nitrogen fixation controlled by iron availability. *Nat. Geosci.* **2**, 867–871 (2009).
15. J. T. Snow, C. Schlosser, E. M. S. Woodward, M. M. Mills, E. P. Achterberg, C. Mahaffey, T. S. Bibby, C. M. Moore, Environmental controls on the biogeography of diazotrophy and *Trichodesmium* in the Atlantic Ocean. *Global Biogeochem. Cycles* **29**, 865–884 (2015).
16. J. A. Sohm, E. A. Webb, D. G. Capone, Emerging patterns of marine nitrogen fixation. *Nat. Rev. Microbiol.* **9**, 499–508 (2011).
17. M. Chen, Y. Lu, N. Jiao, J. Tian, S. J. Kao, Y. Zhang, Biogeographic drivers of diazotrophs in the western Pacific Ocean. *Limnol. Oceanogr.* **64**, 1403–1421 (2019).
18. N. M. Mahowald, A. R. Baker, G. Bergametti, N. Brooks, R. A. Duce, T. D. Jickells, N. Kubilay, J. M. Prospero, I. Tegen, Atmospheric global dust cycle and iron inputs to the ocean. *Global Biogeochem. Cycles* **19**, GB4025 (2005).
19. M. T. Brown, W. M. Landing, C. I. Measures, Dissolved and particulate Fe in the western and central North Pacific: Results from the 2002 IOC cruise. *Geochem. Geophys. Geosyst.* **6**, Q10001 (2005).
20. M. N. W. Grabowski, M. J. Church, D. M. Karl, Nitrogen fixation rates and controls at Stn ALOHA. *Aquat. Microb. Ecol.* **52**, 175–183 (2008).
21. M. Rouco, K. R. Frischkorn, S. T. Haley, H. Alexander, S. T. Dyhrman, Transcriptional patterns identify resource controls on the diazotroph *Trichodesmium* in the Atlantic and Pacific oceans. *ISME J.* **12**, 1486–1495 (2018).
22. T. D. Jickells, Z. S. An, K. K. Andersen, A. R. Baker, G. Bergametti, N. Brooks, J. J. Cao, P. W. Boyd, R. A. Duce, K. A. Hunter, H. Kawahata, N. Kubilay, J. laRoche, P. S. Liss, N. Mahowald, J. M. Prospero, A. J. Ridgwell, I. Tegen, R. Torres, Global iron connections between desert dust, ocean biogeochemistry, and climate. *Science* **308**, 67–71 (2005).
23. A. C. Martiny, M. W. Lomas, W. Fu, P. W. boyd, L. Y. L. Chen, G. A. Cutter, M. J. Ellwood, K. Furuya, F. Hashihama, J. Kanda, D. M. Karl, T. Kodama, Q. P. Li, J. Ma, T. Moutin, E. M. Woodward, J. K. Moore, Biogeochemical controls of surface ocean phosphate. *Sci. Adv.* **5**, eaax0341 (2019).
24. A. N. Knapp, K. L. Casciotti, W. M. Berelson, M. G. Prokopenko, D. G. Capone, Low rates of nitrogen fixation in eastern tropical South Pacific surface waters. *Proc. Natl. Acad. Sci. U.S.A.* **113**, 4398–4403 (2016).
25. S. Bonnet, M. Caffin, H. Berthelot, T. Moutin, Hot spot of N_2 fixation in the western tropical South Pacific pleads for a spatial decoupling between N_2 fixation and denitrification. *Proc. Natl. Acad. Sci. U.S.A.* **114**, E2800–E2801 (2017).
26. T. Shiozaki, K. Furuya, T. Kodama, S. Kitajima, S. Takeda, T. Takemura, J. Kanda, New estimation of N_2 fixation in the western and central Pacific Ocean and its marginal seas. *Glob. Biogeochem. Cycles* **24**, GB1015 (2010).
27. T. Shiozaki, K. Furuya, T. Kodama, S. Takeda, Contribution of N_2 fixation to new production in the western North Pacific Ocean along 155°E. *Mar. Ecol. Prog. Ser.* **377**, 19–32 (2009).
28. L. Y. L. Chen, H. Y. Chen, Y. H. Lin, T. C. Yong, Y. Taniuchi, S. H. Tuo, The relative contributions of unicellular and filamentous diazotrophs to N_2 fixation in the South China Sea and the upstream Kuroshio. *Deep Sea Res.* **85**, 56–71 (2014).
29. T. Shiozaki, S. Takeda, S. Itoh, T. Kodama, X. Liu, F. Hashihama, K. Furuya, Why is *Trichodesmium* abundant in the Kuroshio? *Biogeosciences* **12**, 6931–6943 (2015).
30. J. Wu, S. W. Chung, L. S. Wen, K. K. Liu, L. Y. L. Chen, H. Y. Chen, D. M. Karl, Dissolved inorganic phosphorus, dissolved iron, and *Trichodesmium* in the oligotrophic South China Sea. *Global Biogeochem. Cycles* **17**, 1008 (2003).
31. L. Y. L. Chen, H. Y. Chen, Y. H. Lin, Distribution and downward flux of *Trichodesmium* in the South China Sea as influenced by the transport from the Kuroshio Current. *Mar. Ecol. Prog. Ser.* **259**, 47–57 (2003).
32. W. Mohr, T. Großkopf, D. W. Wallace, J. LaRoche, Methodological underestimation of oceanic nitrogen fixation rates. *PLOS ONE* **5**, e12583 (2010).
33. Y. Lu, Z. Wen, D. Shi, W. Lin, S. Bonnet, M. Dai, S. J. Kao, Biogeography of N_2 fixation influenced by the western boundary current intrusion in the South China Sea. *J. Geophys. Res. Oceans* **124**, 6983–6996 (2019).

34. Y. W. Luo, S. C. Doney, L. A. Anderson, M. Benavides, I. Berman-Frank, A. Bode, S. Bonnet, K. H. Bostrom, D. Bottjer, D. G. Capone, E. J. Carpenter, L. Y. L. Chen, M. J. Church, J. E. Dore, L. I. Falcon, A. Fernandez, R. A. Foster, K. Furuya, F. Gomez, K. Gundersen, A. M. Hynes, D. M. Karl, S. Kitajima, R. J. Langlois, J. LaRoche, R. M. Letelier, E. Maranon, D. J. McGillicuddy, P. H. Moisander, C. M. Moore, B. Mourino-Carballido, M. R. Mulholland, J. A. Needoba, K. M. Orcutt, A. J. Poulton, E. Rahav, P. Raimbault, A. P. Rees, L. Riemann, T. Shiozaki, A. Subramaniam, T. Tyrrell, K. A. Turk-Kubo, M. Varela, T. A. Villareal, E. A. Webb, A. E. White, J. Wu, J. P. Zehr, Database of diazotrophs in global ocean abundance, biomass and nitrogen fixation rates. *Earth Syst. Sci. Data* **4**, 47–73 (2012).
35. T. Shiozaki, T. Kodama, S. Kitajima, M. Sato, K. Furuya, Advective transport of diazotrophs and importance of their nitrogen fixation on new and primary production in the western Pacific warm pool. *Limnol. Oceanogr.* **58**, 49–60 (2013).
36. T. Grosskopf, W. Mohr, T. Baustian, H. Schunck, D. Gill, M. M. Kuypers, G. Lavik, R. A. Schmitz, D. W. Wallace, J. LaRoche, Doubling of marine dinitrogen-fixation rates based on direct measurements. *Nature* **488**, 361–364 (2012).
37. S. Kitajima, K. Furuya, F. Hashihama, S. Takeda, J. Kanda, Latitudinal distribution of diazotrophs and their nitrogen fixation in the tropical and subtropical western North Pacific. *Limnol. Oceanogr.* **54**, 537–547 (2009).
38. M. J. Church, C. Mahaffey, R. M. Letelier, R. Lukas, J. P. Zehr, D. M. Karl, Physical forcing of nitrogen fixation and diazotroph community structure in the North Pacific subtropical gyre. *Global Biogeochem. Cycles* **23**, GB2020 (2009).
39. T. Shiozaki, D. Bombar, L. Riemann, M. Sato, F. Hashihama, T. Kodama, I. Tanita, S. Takeda, H. Saito, K. Hamasaki, K. Furuya, Linkage between dinitrogen fixation and primary production in the oligotrophic South Pacific Ocean. *Global Biogeochem. Cycles* **32**, 1028–1044 (2018).
40. M. R. Gradoville, H. Farnelid, A. E. White, K. A. Turk-Kubo, B. Stewart, F. Ribalet, S. Ferrón, P. Pinedo-Gonzalez, E. V. Armbrust, D. M. Karl, S. John, J. P. Zehr, Latitudinal constraints on the abundance and activity of the cyanobacterium UCYN-A and other marine diazotrophs in the North Pacific. *Limnol. Oceanogr.* **65**, 1858–1875 (2020).
41. J. P. Zehr, D. G. Capone, Changing perspectives in marine nitrogen fixation. *Science* **368**, eaay9514 (2020).
42. P. H. Moisander, R. A. Beinart, I. Hewson, A. E. White, K. S. Johnson, C. A. Carlson, J. P. Montoya, J. P. Zehr, Unicellular cyanobacterial distributions broaden the oceanic N_2 fixation domain. *Science* **327**, 1512–1514 (2010).
43. C. T. Chien, K. R. M. Mackey, S. Dutkiewicz, N. M. Mahowald, J. M. Prospero, A. Paytan, Effects of African dust deposition on phytoplankton in the western tropical Atlantic Ocean off Barbados. *Global Biogeochem. Cycles* **30**, 716–734 (2016).
44. C. Schlosser, J. K. Klar, B. D. Wake, J. T. Snow, D. J. Honey, E. M. S. Woodward, M. C. Lohan, E. P. Achterberg, C. M. Moore, Seasonal ITCZ migration dynamically controls the location of the (sub)tropical Atlantic biogeochemical divide. *Proc. Natl. Acad. Sci. U.S.A.* **111**, 1438–1442 (2014).
45. M. Mills, C. Ridame, M. Davey, J. L. Roche, R. J. Geider, Iron and phosphorus co-limit nitrogen fixation in the eastern tropical North Atlantic. *Nature* **429**, 292–294 (2004).
46. T. J. Browning, E. P. Achterberg, I. Rapp, A. Engel, E. M. Bertrand, A. Tagliabue, C. M. Moore, Nutrient co-limitation at the boundary of an oceanic gyre. *Nature* **551**, 242–246 (2017).
47. T. Weber, C. Deutsch, Local versus basin-scale limitation of marine nitrogen fixation. *Proc. Natl. Acad. Sci. U.S.A.* **111**, 8741–8746 (2014).
48. R. Zhang, X. Zhu, C. Yang, L. Ye, G. Zhang, J. Ren, Y. Wu, S. Liu, J. Zhang, M. Zhou, Distribution of dissolved iron in the Pearl River (Zhujiang) Estuary and the northern continental slope of the South China Sea. *Deep Sea Res.* **167**, 14–24 (2019).
49. T. Shiozaki, T. Nagata, M. Ijichi, K. Furuya, Nitrogen fixation and the diazotroph community in the temperate coastal region of the northwestern North Pacific. *Biogeosciences* **12**, 4751–4764
50. J. P. Montoya, M. Voss, P. Kähler, D. G. Capone, A simple, high-precision, high-sensitivity tracer assay for N_2 fixation. *Appl. Environ. Microbiol.* **62**, 986–993 (1996).
51. T. Hama, S. Kawashima, K. Shimotori, Y. Satoh, Y. Omori, S. Wada, T. Adachi, S. Hasegawa, T. Midorikawa, M. Ishii, S. Saito, D. Sasano, H. Endo, T. Nakayama, I. Inouye, Measurement of photosynthetic production of a marine phytoplankton population using a stable ^{13}C isotope. *Mar. Biol.* **73**, 31–36 (1983).
52. M. J. Church, B. D. Jenkins, D. M. Karl, J. P. Zehr, Vertical distributions of nitrogen fixing phylotypes at Stn ALOHA in the oligotrophic North Pacific Ocean. *Aquat. Microb. Ecol.* **38**, 3–14 (2005).
53. A. W. Thompson, B. J. Carter, K. Turk-Kubo, F. Malfatti, F. Azam, J. P. Zehr, Genetic diversity of the unicellular nitrogen-fixing cyanobacteria UCYN-A and its prymnesiophyte host. *Environ. Microbiol.* **16**, 3238–3249 (2014).
54. M. J. Church, C. M. Short, B. D. Jenkins, D. M. Karl, J. P. Zehr, Temporal patterns of nitrogenase gene (*nifH*) expression in the oligotrophic North Pacific Ocean. *Appl. Environ. Microbiol.* **71**, 5362–5370 (2005).
55. P. H. Moisander, R. A. Beinart, M. Voss, J. P. Zehr, Diversity and abundance of diazotrophic microorganisms in the South China Sea during intermonsoon. *ISME J.* **2**, 954–967 (2008).
56. H. Farnelid, K. Turk-Kubo, M. C. Muñoz-Marín, J. P. Zehr, New insights into the ecology of the globally significant uncultured nitrogen-fixing symbiont UCYN-A. *Aquat. Microb. Ecol.* **77**, 125–138 (2016).
57. J. Ma, D. X. Yuan, Y. Liang, M. H. Dai, A modified analytical method for the shipboard determination of nanomolar concentrations of orthophosphate in seawater. *J. Oceanogr.* **64**, 443–449 (2008).
58. J. Z. Zhang, Shipboard automated determination of trace concentrations of nitrite and nitrate in oligotrophic water by gas-segmented continuous flow analysis with a liquid waveguide capillary flow cell. *Deep Sea Res.* **47**, 1157–1171 (2000).
59. D. W. King, H. A. Lounsbury, F. J. Millero, Rates and mechanism of Fe(II) oxidation at nanomolar total iron concentrations. *Environ. Sci. Technol.* **29**, 818–824 (1995).
60. M. E. Lagerstrom, M. P. Field, M. Seguret, L. Fischer, S. Hann, R. M. Sherrell, Automated on-line flow-injection ICP-MS determination of trace metals (Mn, Fe, Co, Ni, Cu and Zn) in open ocean seawater: Application to the GEOTRACES program. *Mar. Chem.* **155**, 71–80 (2013).
61. J. R. Ledwell, A. J. Watson, C. S. Law, Evidence for slow mixing across the pycnocline from an open-ocean tracer-release experiment. *Nature* **364**, 701–703 (1993).

Acknowledgments: We thank S.-J. Kao, W. Zou, and L. Tian for technical assistance with the analysis of POC and PON and their isotopic composition. We also thank L. Wang, J. Liu, and Y. Zhou for help with nutrient and dFe analysis. We acknowledge the captain and crew of the R/V *Tan Kah Kee* for the help during the cruises. **Funding:** This work was supported by the National Science Foundation of China (41925026, 41890802, 31861143022, 42076149, 41890801, 41876081, and 41721005) and the XPLORER Prize from the Tencent Foundation to D.S. **Author contributions:** D.S., Z.W., and M.D. designed the research. Z.W., Y.C., R.D., R.Z., R.J., and W.L. performed the experiments. Z.W., T.J.B., D.S., C.D., X.L., Z.C., and H.H. analyzed the data. Z.W., T.J.B., and D.S. wrote the manuscript. All authors discussed the results and commented and edited the manuscript. **Competing interests:** The authors declare that they have no competing interests. **Data and materials availability:** All data needed to evaluate the conclusions in the paper are present in the paper and/or the Supplementary Materials. Additional data related to this paper may be requested from the authors.

Submitted 3 August 2021
Accepted 14 December 2021
Published 4 February 2022
10.1126/sciadv.abl7564

ScienceAdvances

Nutrient regulation of biological nitrogen fixation across the tropical western North Pacific

Zuozhu WenThomas J. BrowningYihua CaiRongbo DaiRuifeng ZhangChuanjun DuRuotong JiangWenfang LinXin LiuZhimian CaoHaizheng HongMinhan DaiDalin Shi

Sci. Adv., 8 (5), eabl7564. • DOI: 10.1126/sciadv.abl7564